ISFV13 - 13th International Symposium on Flow Visualization
FLUVISU12 - 12th French Congress on Visualization in Fluid Mechanics
July 1-4, 2008, Nice, France

# VISUALIZING THE FLOW INDUCED BY AN AIR CURTAIN USING STEREO PARTICLE IMAGE VELOCIMETRY

**Frank K. Lu, Adam J. Pierce**
**University of Texas at Arlington, Arlington, Texas 76019, USA**

KEYWORDS:
**Main subject(s):** *Environmental flow*
**Fluid:** *Aerodynamics*
**Visualization method(s):** *Stereo particle image velocimetry*
**Other keywords:** *Air curtain*

ABSTRACT: *A stereo particle image velocimetry technique was developed to study the flow of a commercial, off-the-shelf air curtain. Surveys were performed along lengthwise planes only. The flow leaving the air curtain was highly turbulent with turbulent intensities as high as 20 percent based on the maximum jet velocity. The jet from the air curtain did not show much spreading in the lengthwise planes. The turbulence level decreased as the flow progressed toward the floor. Upon reaching the floor vents, the turbulence level rose again.*

## 1 Introduction

One of the main uses of air curtains is to provide a dynamic barrier that allows for easy movement of people and materials between large enclosed spaces. Nonetheless, despite the ubiquity of air curtains in the urban landscape, there does not appear to be much detailed study of these devices until recently. These detailed studies made use of advances in nonintrusive, mapping techniques and numerical modeling [1–6].

Fundamentally, air curtain flows fall into the category of a rectangular jet which does not have a large, two-dimensional region as in the case of a planar jet. According to [7–10], a planar jet can only be achieved for aspect ratios that may be as high as 60, a requirement that is not typically found in air curtains. Additional complications of air curtains are that the flow may be transitional and typically have high initial turbulence levels. To further the understanding of such air flows, a detailed mapping of the flow from a commercial air curtain using stereo particle image velocimetry was performed. The mean and turbulent properties of the flow were analyzed. This paper reports some preliminary visualization results confined to lengthwise planes only.

## 2 Experimental Method

### 2.1 Facility

The test facility comprised of a 2.4 $m^3$ cabin partitioned by a 0.15 m thick wall, as shown schematically in Fig. 1. The facility was raised 0.6 m from the laboratory floor to accommodate ducting. A 0.91 m

wide × 2.1 m high opening connected the two chambers. On top of the doorway was mounted a commercial air curtain (Fantech Model AC3600). According to the air curtain manufacturer, the maximum flow velocity is 10.3 m/s and the maximum flow rate is 22.5 $m^3$/min. The exhaust of the air curtain was directed through a grilled vent comprising of a grid of six rows of 25 rectangular openings, each 30 mm long by 10 mm wide, totaling 0.0444 $m^2$. The entire air curtain exhaust housing can be swiveled but it was set to nominally deliver a vertical air curtain downward.

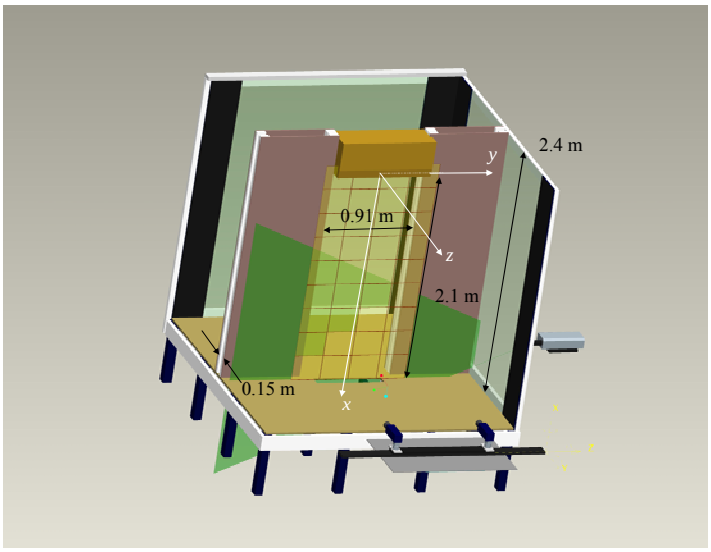


Fig. 1. Cutaway view of test cabin.

The air curtain was modified to accept flow from a wide-angle diffuser. A number of guide vanes set equidistant apart from each other were placed in the diffuser to condition the flow. The flow itself was produced by a fan in the air curtain and captured by two floor vents directly below the air curtain and separated from each other by 25.4 mm. The vents were covered by registers, each 101.6 wide by 304.8 mm long. The total open area of the floor vents was approximately equal to the open area of the air curtain exhaust vent in order to match the air curtain's exhaust area. Upon passing the floor vent, the air entered a 0.0084 $m^3$ plenum. The air then traveled through a 305 mm diameter air conditioning duct which redirected it to the cabin's roof, entering the diffuser which was located approximately 3.5 ft behind the air curtain unit. Next, the air passed through the diffuser to smooth the air flow. After the diffuser, the air traveled back to the front portion of the air curtain as mentioned above. An airtight circulation system was thus set up. The air curtain fixture was offset to one side of the doorway to enable the bulk of the flow to be mapped by the SPIV technique.

## 2.2 SPIV System

A LaVision FlowMaster 3D SPIV system was used in this study. A pencil of light at a wavelength of 532 nm from a New Wave Research Solo 120 Nd:YAG double-pulsed laser was spread into a 2.5 mm thick sheet by a cylindrical lens with a focal length of $f = -10$ mm. This allowed a working distance of 2 m which fulfilled the distance requirement needed for the laser to properly illuminate the measurement area. For the present experiments, the lasers were pulsed at 5 Hz at 2 × 120 mJ/pulse, with a pulse duration of 11 ms. The images were captured by two Flow Master 3S ImagerIntense/ImagePro ICCD cameras with 1376 × 1040 pixel resolution and a 12 bit dynamic range. A frame grabber, control electronics and a computer with dual Intel Xeon processors running the DaVis 7.1 PIV data acquisition and processing software were other major components of the imaging system. Data were stored in a 750 GB hard drive.

Extra virgin olive oil was atomized by a LaVision V-Z Droplet Seeder to produce droplets with an estimated mean diameter of 1 μm. The seeder was run for 15 s with the air curtain turned on. The air curtain was run for another minute to distribute the seed material. Sufficient seed material was then produced without saturating the cameras. The concentration decreased as the oil droplets became

absorbed to the wooden structure and through tiny leaks. Sufficient seed was available for 45 minutes which was sufficient for surveying an entire plane.

## 2.3 Experimental Procedure

All the surveys reported here were in vertical planes parallel to the doorway. Surveys in the transverse plane are not reported for brevity. The laser sheet was aligned by using a low-powered Sears Craftsman 180° precision laser level.

The cameras were mounted on a lift system that allowed them to be aligned parallel with the survey planes using the so-called lateral displacement configuration [11]. A photograph of the camera lift system is shown in Fig. 2, where the two cameras are shown located at the top of the lift. The two cameras were at a fixed separation distance of 815 mm from each other. They rested on a 100 cm optical rail which was mounted on another 300 cm rail. The camera axes subtended the same angle with the light sheet.

Fig. 2. Photograph of the front of the test cabin showing the lifting mechanism for the stereo cameras.

Six planes were surveyed. The first plane was located at the longitudinal axis of the air curtain, this being 1846.5 mm from the cameras' focal plane. The other planes were located at 95.5, 76, 75, 154 and 151 mm from the previous plane toward the cameras, respectively. Details of each plane, including other information to be discussed later, are found in Table 1. The survey planes encompassed the air curtain. The camera separation of 815 mm yielded a half-angle between the cameras and the center of the image of 12.45 to 17.46°, which was within the recommendations of Prasad [11], thereby minimizing off-axis error in the horizontal plane. Only a small common area can be captured by the pair of cameras. Therefore, a survey of an entire

Table 1. Rows and rectangles per survey plane.

| Plane | Location of plane from camera plane (mm) | No. of rows and rectangles | Size of individual rectangle ($mm^2$) | Total image size ($m^2$) |
|---|---|---|---|---|
| 1 | 1846.5 | 9 × 4 | 278.8 × 195.2 | 1.171 × 1.952 |
| 2 | 1751.0 | 9 × 4 | 266.2 × 186.3 | 1.091 × 1.863 |
| 3 | 1675.0 | 10 × 4 | 254.2 × 178.9 | 1.068 × 1.982 |
| 4 | 1600.0 | 10 × 4 | 243.9 × 170.7 | 1.000 × 1.927 |
| 5 | 1446.0 | 11 × 4 | 217.1 × 152.0 | 0.912 × 1.737 |
| 6 | 1295.0 | 12 × 5 | 194.1 × 136.4 | 1.150 × 1.949 |

plane necessitated the patching together of a number of ensemble-averaged images of individual common areas. This is shown schematically in Fig. 1 by an array of rectangles covering the doorway. The actual distribution of these rectangles is found in Table 1. The image area decreased nearer to the camera due to perspective. For example, Plane 1, which was most distant from the cameras, comprised of nine rows of four rectangles, each rectangle being 308 mm wide by 277 mm high, to provide a coverage of 1.23 m wide and 2.22 m high.

Four hundred stereo images were taken at each location in order to obtain ensemble averaged statistics for the mean and turbulent flow quantities, as compared to 150 images [14] and 500 images [1]. This number of images was found to be the minimum number for obtaining reliable turbulence statistics although 150 images were sufficient for mean velocity values. After obtaining the 400 stereo images, the cameras were then translated horizontally to obtain images from the next rectangle, and so forth. This process was repeated until data for an entire row were collected. Once a given row was completed, the cameras were then moved to the next height and the data gathering process was repeated. The entire dataset for one plane was then processed by DaVis to yield ensemble statistics of the velocity field. DaVis merged the data of each rectangle to yield a map of the entire plane. The topmost row (No. 8) was designated as the datum row. The entire process of acquiring the SPIV images and processing the data for each plane took about 16 hours.

#### *2.3.1 Position Uncertainty*

The major concern regarding uncertainty is the position of the interrogation region. The laser sheet should be vertical and thin, while its inclination is of minor importance (within reasonable limits) so long as the sheet covers the interrogation region. The use of the laser level allowed the Nd:YAG laser sheet to be aligned vertically and perpendicularly to the side of the cabin.

Vertical coverage was achieved by lifting the entire imaging system up and down on a warehouse lift (Genie Superlift™ Advantage Model SLA-15), as shown in Fig. 2. A precise alignment to ±1 mm (based on the accuracy of the rail mount) in the $x$, ±2 mm in $y$ and ±3 mm in the $z$ direction, respectively, was achieved. The distance in the $z$ direction was obtained using a Leica Disto A3 Laser Distancemeter. This laser measuring device is capable of measuring from a range of 0.05 m to 100 m. There was negligible rotation of the imaging system. Finally, the angled views of the two cameras produced perspective distortions which can be compensated via calibration [12,13]. The small angle subtended between the two cameras to the center of the image caused a larger uncertainty in the $z$ direction. Prasad [11] indicated that the out-of-plane error exceeds the in-plane error by a factor of 3 to 4, namely, $\Delta z < 3$ mm, which is on the same order as the laser sheet thickness of 2.5 mm. The cameras can be located to better than $\pm 0.25$ mm on the rails. In conclusion, the uncertainties in the images are $\Delta x \approx 1$ mm, $\Delta y \approx 2$ mm and $\Delta z \approx 4$ mm.

## 3 Results

### 3.1 Streamlines

The ensemble-averaged streamlines of all six planes are shown in Fig. 3, where the location of the doorway is indicated by a yellow frame. The figures show a distinct mean downward flow in plane 1 that appears slightly inclined to the left. The reason for this slight inclination is not known but it may

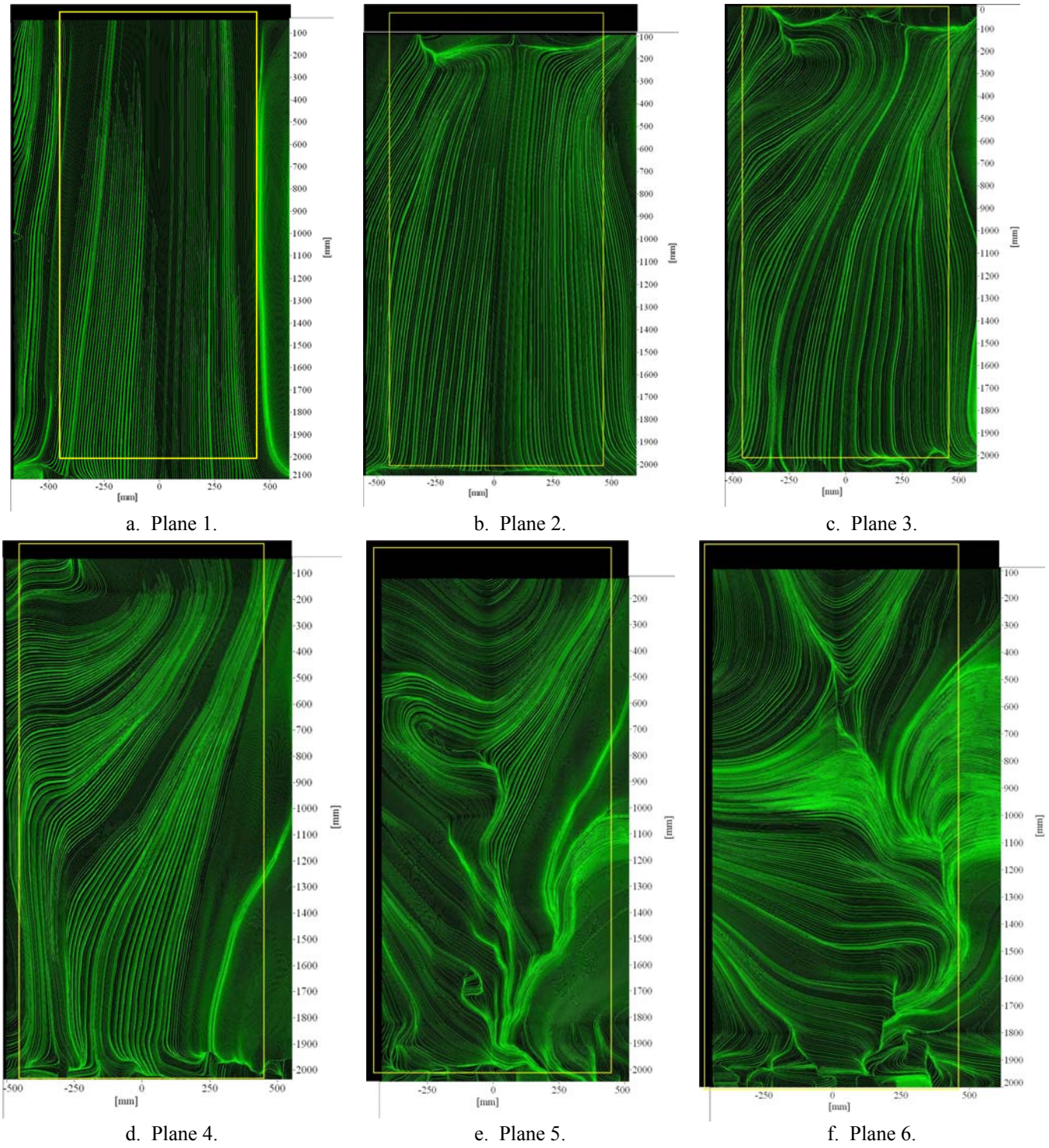


a. Plane 1. b. Plane 2. c. Plane 3.

d. Plane 4. e. Plane 5. f. Plane 6.

Fig. 3. Ensemble-averaged streamline patterns.

be due to the air curtain unit being mounted slightly to the left of the doorway to accommodate its motor and switch. It may also be due to the slightly nonuniform flow leaving the air curtain. The streamline pattern progressively deteriorated as one progressively moves away from the air curtain and became unrecognizable by plane 4. The streamline patterns for Planes 5 and 6 were erratic and were

actually extremely weak flows that cannot be adequately resolved by the SPIV system. Hence, subsequent discussion will ignore these last two planes.

### 3.2 Velocity Profiles

The ensemble-averaged, in-plane velocity maps are shown in Fig. 4. The figure shows a jet with a well-defined edge for most of plane 1. The jet velocity decreases rapidly for the other planes. The transverse growth of the jet is evident in plane 2 where the velocity values are higher further away from the air curtain exhaust. This is because plane 2 intersects the growing jet at some distance from the exhaust.

The ensemble-averaged velocities at selected locations for plane 1 are displayed in Fig. 5. In the figures, the long dashed lines represent the sides of the doorway locations. Figure 5 shows that the jet left the air curtain with a slightly distorted initial profile in $u$, the longitudinal velocity component. However, the velocity distribution showed improved symmetry at $x > 400$ mm. The jet spread gently and displayed an asymmetry, with a slightly higher velocity toward the left. This asymmetry may be due to the slightly asymmetric mounting of the air curtain over the doorway. The figure also shows that the maximum value of $u$ decreased to nearly stagnation at the floor. The presence of the two floor vents is also evident in the axial velocity profile closest to the floor. Finally, Fig. 5 shows a negligible transverse velocity component in the middle portion of the jet. The transverse components were more significant at the edges of the jet but the values were small compared to the axial component. Toward the floor, the ($\underline{v}$, $\underline{w}$) components showed that the flow was channeled into the vents.

The shearing at the edges of the air curtain is evident in the high values of the transverse vorticity as shown in Fig. 6. The high values were confined to two narrow regions near the exit of the air curtain. The left edge showed a longer region of vorticity than the right, due to the slightly asymmetric jet. These regions promoted entrainment of the ambient air into the air curtain.

Figure 7 shows the turbulence kinetic energy and the three Reynolds stress components. As mentioned in the Introduction, air curtains generally have high levels of turbulence. This feature is also manifested in the present results. The turbulence intensity $\sqrt{\overline{u'^2}}/\overline{u}_{max}$ was of the order of 20% of the maximum jet velocity upon leaving the air curtain. However, the turbulence damped out at $x \approx 1000$ mm. The turbulence level remained higher at the edges of the jet due to mixing with the ambient. The high level of turbulence was also reflected in the unsteadiness of the frame-to-frame PIV data. An example of this is shown in Fig. 8 for a region at the middle of the left edge of the air curtain. A video showing this unsteadiness is available with the paper. Large, unsteady flow structures are evident in the figure. These disappeared in the ensemble-averaged plots of Fig. 4. Finally, the turbulence increased at the floor as the jet impinged on the registers covering the two vents.

## 4 Conclusions

The flow from a commercial, off-the-shelf air curtain was visualized using stereo particle image velocimetry. An innovative approach was implemented to survey the large area. Ensemble averages were taken to obtain statistical properties of the flow. The study showed a highly turbulent planar jet exiting the curtain. The high level of turbulence is attributed to the grilled exhaust. The study also showed that the jet did not show much spreading. The turbulence level was reduced as the flow progressed toward the floor. Upon reaching the floor vents, the turbulence level rose again.

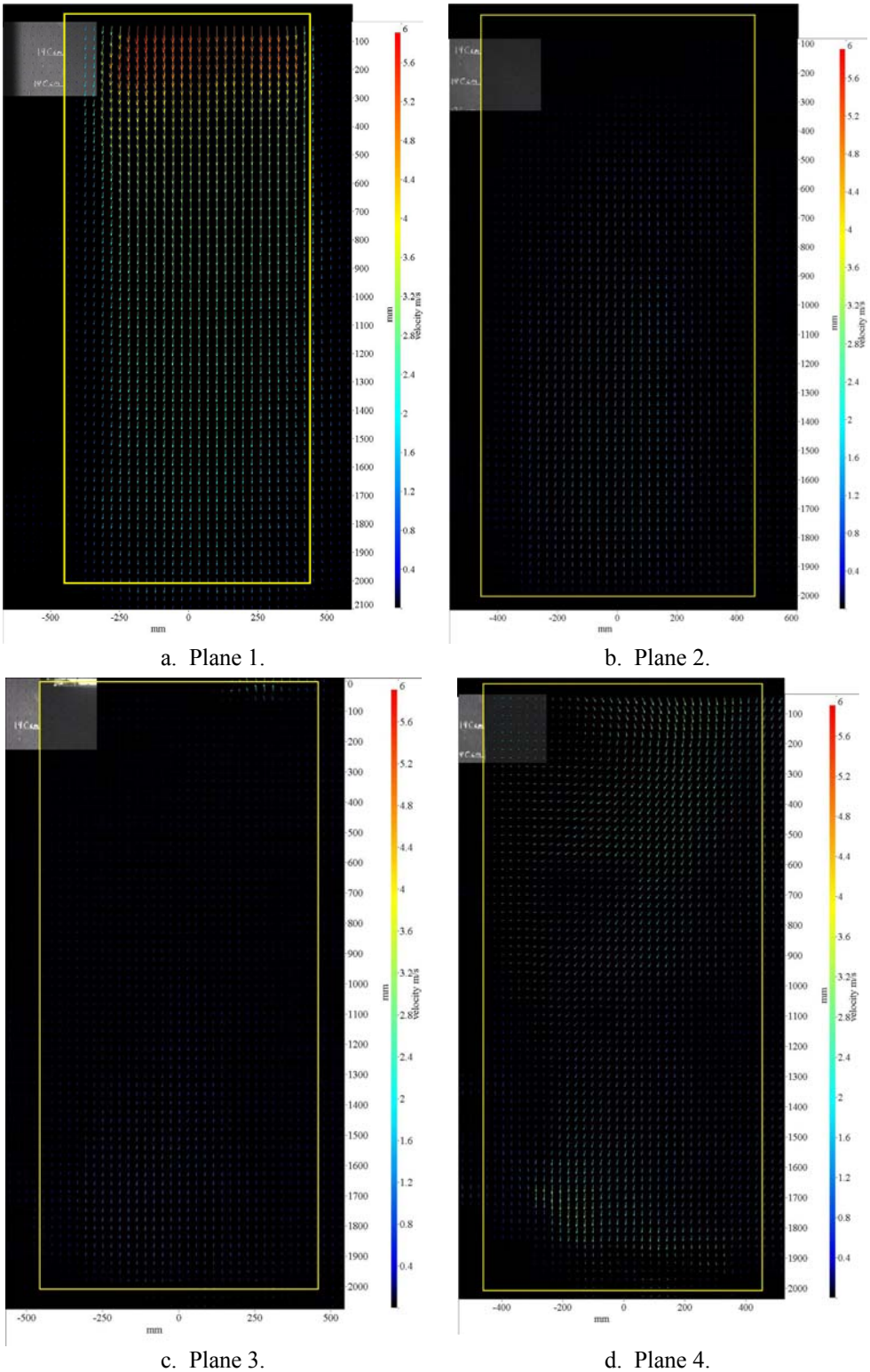


a. Plane 1. b. Plane 2.

c. Plane 3. d. Plane 4.

Fig. 4. Ensemble-averaged velocity maps.

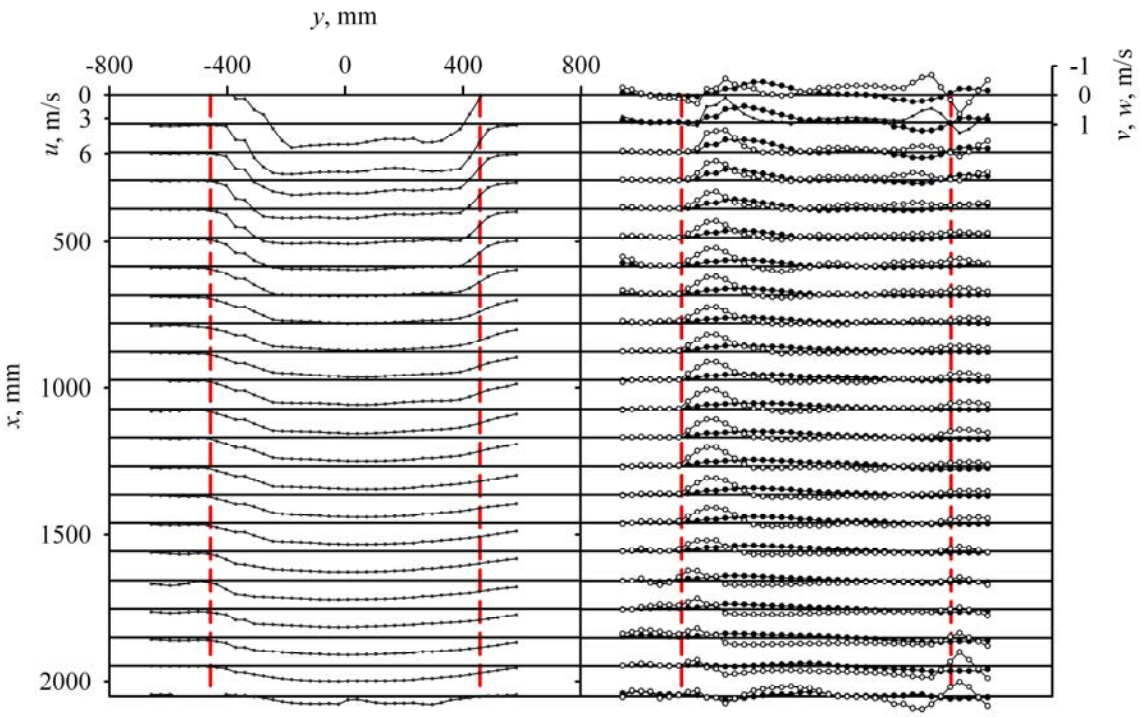


Fig. 5. Ensemble-averaged velocity distributions for plane 1.

## 5 Acknowledgements

Funding for the SPIV system was a National Science Foundation's Major Research Instrument Grant (No. 0421282). The authors acknowledge the assistance of Vijay Chauhan and Linda Phonharath in the initial stages of the work, as well as the advice of Prof. J. Craig Dutton.

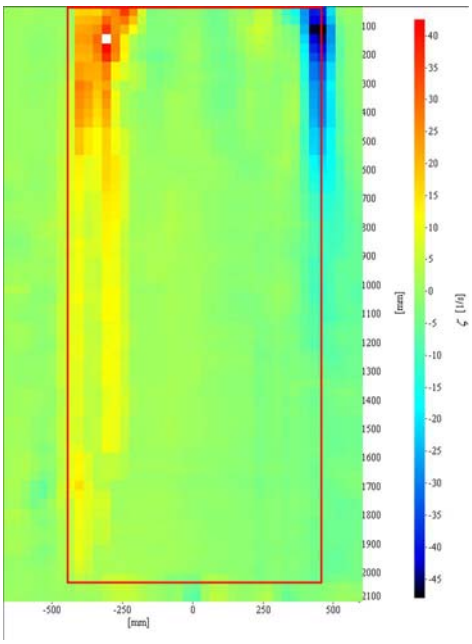

Fig. 6. Vorticity distribution for plane 1.

## References

1. Field BS and Loth E. An air curtain along a wall with high inlet turbulence. *Journal of Fluids Engineering*, Vol. 126, No. 3, pp 391–398, 2004.
2. Bhattacharjee P and Loth E. Simulations of laminar and transitional cold wall jets. *International Journal of Heat and Fluid Flow*, Vol. 25, No. 1. pp 32–43, 2004.
3. Cui J and Wang S. Application of CFD in evaluation and energy-efficient design of air curtains for horizontal refrigerated display cases. *International Journal of Thermal Sciences*, Vol. 43, No. 10, pp 993–1002, 2004.

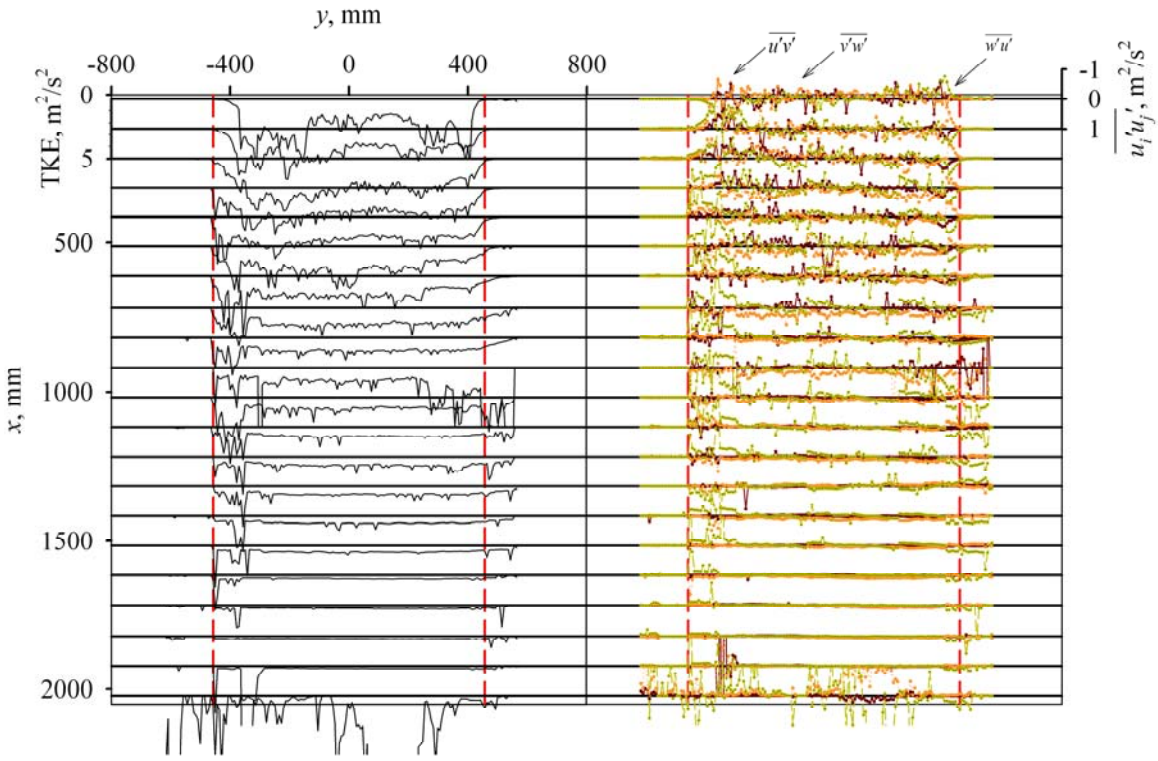


Fig. 7. Ensemble-averaged turbulence kinetic energy and Reynolds stress components for plane 1.


4. Chen Y-G, Yuan X-L. Experimental study of the performance of single-band air curtains for a multi-deck refrigerated display cabinet. *Journal of Food Engineering*, Vol. 69, No. 3, pp. 261–267, 2005.
5. Costa JJ, Oliveira LA and Silva MCG. Energy savings by aerodynamic sealing with a downward-blowing plane air curtain—a numerical approach. *Energy and Buildings*, Vol. 38, No. 10, pp 1182–1193, 2006.
6. Neto LPC, Silva MCG and Costa JJ. On the use of infrared thermography in studies with air curtain devices. *Energy and Buildings*, Vol. 38, No. 10, pp. 1194–1199, 2006.
7. D'Agaro P, Cortella G and Croce G. Two- and three-dimensional CFD applied to vertical display cabinets simulation. *International Journal of Refrigeration*, Vol. 29, No. 2, pp 178–190, 2006.
8. Quinn WR. Turbulent free jet flows issuing from sharp-edged rectangular slots: The influence of slot aspect ratio. *Experimental Thermal and Fluid Science*, Vol. 5, No. 2, pp. 203–215, 1992.
9. Mi J, Deo RC, Nathan GJ. Characterization of turbulent jets from high aspect-ratio rectangular nozzles. *Physics of Fluids*, Vol. 17, No. 6, 068102, 2005.
10. Deo RC, Mi J, Nathan GJ. The influence of nozzle aspect ratio on plane jets. *Experimental Thermal and Fluid Science*, Vol. 31, No. 8, pp. 545–559, 2007.
11. Deo, RC, Nathan, GJ, Mi J. Comparison of turbulent jets issuing from rectangular nozzles with and without sidewalls, *Experimental Thermal and Fluid Science*, Vol. 32, No. 2, 596–606, 2007.
12. Prasad AK. Stereoscopic particle image velocimetry. *Experiments in Fluids*, Vol. 29, No. 2, pp. 103–106, 2000.
13. Soloff S, Adrian RJ, Liu ZC. Distortion compensation for generalized stereoscopic particle image velocimetry. *Measurement Science and Technology*, Vol. 8, No. 12, pp. 1441–1454, 1997.

14. Zang W, Prasad AK. Performance evaluation of Scheimpflug stereocamera for particle image velocimetry. *Applied Optics*, Vol. 36, No. 33, pp. 8738–8744, 1997.
15. Rouaud O, Havet M, Solliec C. Influence of external perturbations on a minienvironment: Experimental investigations. *Building and Environment*, Vol. 39, No. 7, pp. 863–872, 2004.

## Copyright Statement

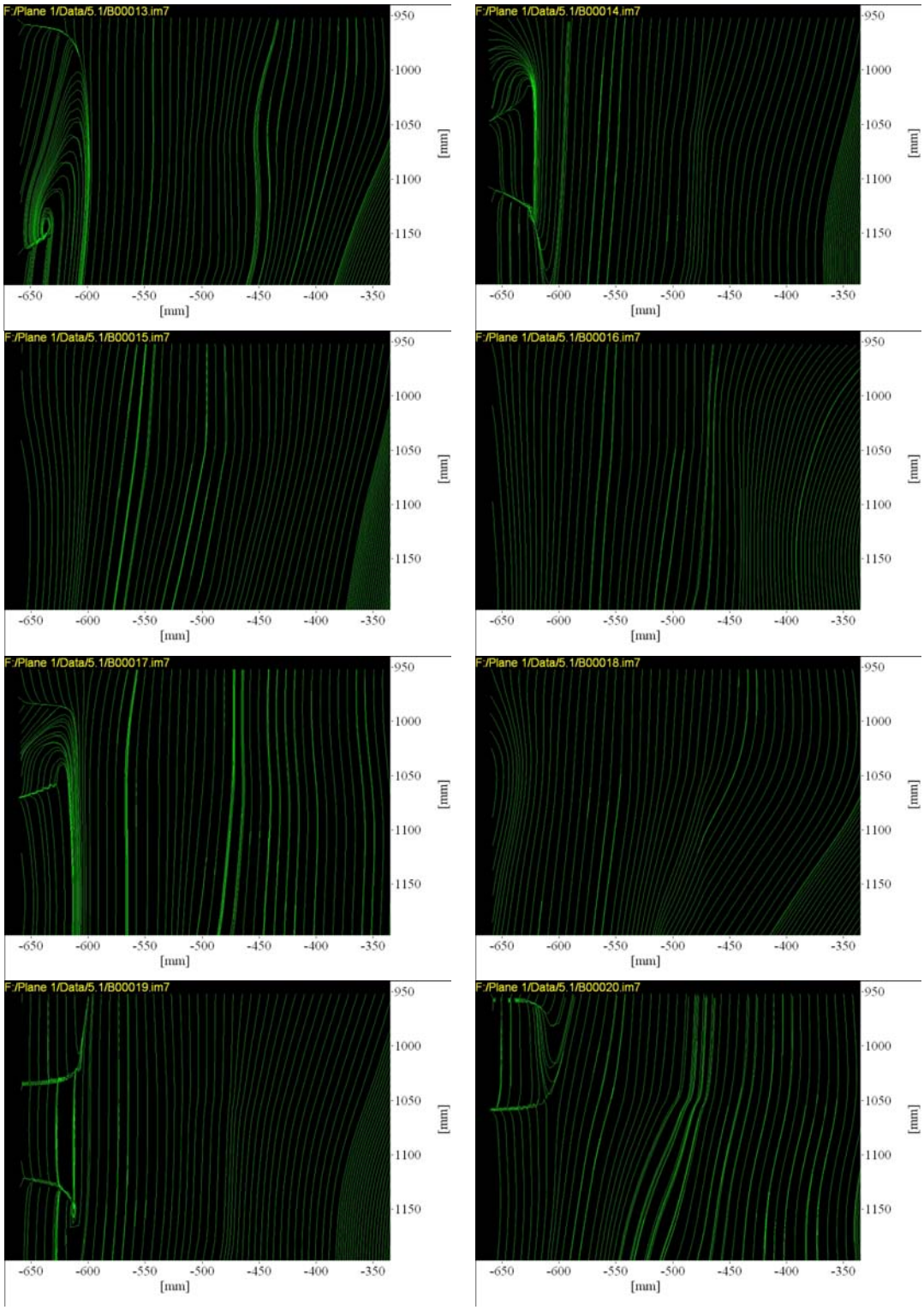


Fig. 8. Sequence of consecutive streamline plots near the middle, left edge of the air curtain.